Journal of Machine Engineering, 2023, Vol. 23, No. 1, 133–153
ISSN 1895-7595 (Print) ISSN 2391-8071 (Online)

Received: *14 December 2022* / Accepted: *01 February 2023* / Published online: *03 February 2023*

multi-objective optimization,
machine learning,
AISI 4340, NSGA-II, ANN

Anh-Tu NGUYEN[1]
Van-Hai NGUYEN[2,3*]
Tien-Thinh LE[2,3]
Nhu-Tung NGUYEN[4]

A HYBRIDIZATION OF MACHINE LEARNING AND NSGA-II FOR MULTI-OBJECTIVE OPTIMIZATION OF SURFACE ROUGHNESS AND CUTTING FORCE IN AISI 4340 ALLOY STEEL TURNING

This work focuses on optimizing process parameters in turning AISI 4340 alloy steel. A hybridization of Machine Learning (ML) algorithms and a Non-Dominated Sorting Genetic Algorithm (NSGA-II) is applied to find the Pareto solution. The objective functions are a simultaneous minimum of average surface roughness (Ra) and cutting force under the cutting parameter constraints of cutting speed, feed rate, depth of cut, and tool nose radius in a range of 50–375 m/min, 0.02–0.25 mm/rev, 0.1–1.5 mm, and 0.4–0.8 mm, respectively. The present study uses five ML models – namely SVR, CAT, RFR, GBR, and ANN – to predict Ra and cutting force. Results indicate that ANN offers the best predictive performance in respect of all accuracy metrics: root-mean-squared-error (RMSE), mean-absolute-error (MAE), and coefficient of determination (R^2). In addition, a hybridization of NSGA-II and ANN is implemented to find the optimal solutions for machining parameters, which lie on the Pareto front. The results of this multi-objective optimization indicate that Ra lies in a range between 1.032 and 1.048 μm, and cutting force was found to range between 7.981 and 8.277 kgf for the five selected Pareto solutions. In the set of non-dominated keys, none of the individual solutions is superior to any of the others, so it is the manufacturer's decision which dataset to select. Results summarize the value range in the Pareto solutions generated by NSGA-II: cutting speeds between 72.92 and 75.11 m/min, a feed rate of 0.02 mm/rev, a depth of cut between 0.62 and 0.79 mm, and a tool nose radius of 0.4 mm, are recommended. Following that, experimental validations were finally conducted to verify the optimization procedure.

1. INTRODUCTION

AISI 4340 alloy steel has low-to-medium carbon content, high strength, and high toughness. Its advantageous properties are a good balance of strength, wear resistance, and toughness. AISI 4340 is categorized among hard-to-cut materials. However, this alloy tends to be used for machining [1]. AISI 4340 alloy steel is widely used in aircraft and automobiles,

[1] Faculty of Mechanical Engineering, Hanoi University of Industry, Bac Tu Liem District, Ha Noi, Vietnam
[2] Faculty of Mechanical Engineering and Mechatronics, Phenikaa University, Yen Nghia, Ha Dong, Ha Noi, Vietnam
[3] PHENIKAA Research and Technology Institute (PRATI), A&A Green Phoenix Group JSC, No. 167 Hoang Ngan, Trung Hoa, Cau Giay, Ha Noi, Vietnam
[4] HaUI Institute of Technology, Hanoi University of Industry, Bac Tu Liem District, Ha Noi, Vietnam
[*] E-mail: hai.nguyenvan1@phenikaa-uni.edu.vn
https://doi.org/10.36897/jme/160172

among other applications. It is also used to manufacture structural parts like gears, shafts, bearings, cams, axles, spindles, couplings, and more, which require a long service life, high tolerance, and high surface quality [2]. Turning is an essential process in the manufacture of such products. In the turning process, the judicious selection of process parameters affects the indexes of cutting efficiency, cost, productivity, and product quality and is closely related to the levels of energy consumption and CO_2 emissions. Therefore, awareness of the relationship of machining parameters is essential in improving overall system performance, such as efficiency, cost, and environmental impact [3]. Consequently, optimization of the process parameters in the machining process is the scientific problem to be solved in the context of green and sustainable production.

In general, the quality of the turning operation is determined by machining tolerance and surface roughness, which customers demand for machined parts [4]. In the turning operation, factors that significantly influence surface roughness are the material and geometry of the tool, nose radius, cutting speed, feed rate, and depth of cut [5]. To achieve a good surface finish for turned components, manufacturers can often use a higher cutting speed, good insert geometry, a suitable nose radius, and a low feed rate. However, the characteristic performance of turning involves not only improving surface quality but also reducing energy consumption in the industrial production process [6]. Cutting power, and cutting forces, are directly impacted by material removal rate and basic cutting parameters (i.e., cutting speed, feed rate, and depth of cut). One of the goals of optimizing the machining process is to reduce machining time. One way to do this is to increase the material removal rate, i.e., increase the cutting parameters [7]. However, this leads to increased cutting force and poorer surface quality. Thus, there is uncertainty in selecting cutting parameters to achieve criteria such as good surface quality, fast machining time, and low energy consumption [8]. In order to solve this problem, it is necessary to determine the optimum combination of parameters to improve machining performance. Therefore, optimizing cutting force and surface roughness is essential for sustainable production, covering energy consumption, machining cost, product quality, and eco-friendly manufacturing [9].

Optimization algorithms – especially evolutionary computing or meta-heuristic techniques – have been applied to determine the optimal cutting conditions to achieve the best machining performance. In cutting parameter optimization, multi-objective techniques have been proposed, which take a number of competing goals into account [10]. Examples include PSO [11], GA [12], artificial bee colony (ABC) [13], non-dominated sorting genetic algorithm (NSGA-II) [14–15], etc. These approaches have been shown to be more robust and accurate in solving complicated engineering problems than traditional optimization methods [16]. Of particular importance is that these approaches can optimize several objectives simultaneously [17–20].

Many recent studies use a hybridization of machine-learning models and optimization algorithms to find the optimal process parameters for performance characteristics. For instance, Bouacha et al. [14] investigated two hybrid models – namely PSO-ANN and NSGA-II-RSM – in the hard turning of AISI 52100 steel. The results showed that the ANN model yielded a more accurate predictive performance than the RMS model, and NSGA-II exhibited better performance than PSO. Furthermore, Yang et al. [21] used NSGA-II and multi-objective differential evolution (MODE) to achieve the optimal process parameters with tool

wear and maximum material removal rate (MRR) in the EN24 steel turning process. Results indicated that NSGA-II performs better than MODE. In order to model and optimize MRR and Ra in grinding operations, Unune et al. [22] integrated NSGA-II with ANN. Judging by the results, NSGA-II is a multi-objective optimization technique that works with a population of points and is quite effective.

Recently, the study on the turning of AISI 4340 steel in terms of optimization of the process parameters focuses on the mathematical model and single-objective optimization [23–27]. There are few studies on multi-objective optimization in AISI 4340 alloy steel turning. In order to bridge the gap in the literature, the present work aims to find the optimum turning parameters that simultaneously deliver minimum surface roughness and minimum cutting force. In this work, the five ML models – namely SVR, CAT, RFR GBR, and ANN – are used to develop the predictive model for surface roughness and cutting force in the AISI 4340 turning process. Then, five ML models are compared for accuracy using the RMSE, MAE, and R^2 metrics to determine which model has the best prediction performance. In order to determine the optimum process parameters that concurrently satisfy the two requirements of minimum Ra and minimum cutting force, the best ML model and NSGA-II algorithm are combined.

2. EXPERIMENTAL SETUP AND DESIGN OF EXPERIMENTS

2.1. EXPERIMENTAL DESIGN

This study used the data reported in the literature [25]. The experiments were performed on a MTAB MAXTURN CNC lathe, whose spindle speed and feed rate can reach 6,000 rpm and 30 m/min. The workpiece was a cylindrical bar of AISI 4340 alloy steel with a Brinell hardness number of 217, a length of 100 mm, and a diameter of 24 mm. The chemical composition of the workpiece is Fe 95.80%, Ni 1.3%, Cr 1.15%, Mn 0.59%, C 0.421%, Mo 0.228%, Si 0.216%, S 0.0278%, according to the manufacturer. The tungsten-coated carbide CCMT-090308 was mounted on the right-hand side of the cutting holder of grade K-10. In the machining process, a mixture of 0.2% multiwalled carbon nanotubes and ethylene glycol was employed as minimum quantity lubrication (MQL), with a pressure of 5 bars and flow rate of 140 ml/hr. In order to perform the experiments, the following process parameters were selected: cutting speed (75 and 90 m/min), feed rate (0.04, 0.06, 0.08, 0.1, and 0.12 mm/rev), depth of cut (0.4 and 0.8 mm), and tool nose radius (0.4 and 0.8 mm). Therefore, sixty experimental runs were conducted throughout the process. The resulting performance characteristics were collected by measurement devices. The cutting conditions are shown in Table 1.

After each experimental run, the machined part was measured three times by the MITUTOYO-Surftest SJ-210P Portable-Surface-Roughness-Tester (Japan). The average value of the three measurements is taken as an experimental result. Cutting forces were measured by the Kistler Dynamometer system. The output signals were amplified and then displayed through laptop and DynoWare software. Table 2 shows the process parameters versus measured results for Ra and cutting force on the 60 experimental runs.

Table 1. Cutting parameters

Cutting factor	Unit	Data levels
Cutting speed, (*Vc*)	mm/min	75, 90
Feed rate, (*f*)	mm/rev	0.04, 0.06, 0.08, 0.10, 0.12
Depth of cut, (*a*)	mm	0.5, 1.0, 1.5
Tool radius nose, (*r*)	mm	0.4, 0.8
Cutting tool, (*T*)		CCMT-090308/K-10
Coolant, (*H*)		MQL 0.2% multiwalled carbon nanotube and ethylene glycol

Table 2. Machining settings used in the experiment [25]

No.	Cutting Speed (m/min)	Nose Radius (mm)	Feed Rate (mm/rev.)	Depth of Cut (mm)	Ra (μm)	Force (kgf)	No.	Cutting Speed (m/min)	Nose Radius (mm)	Feed Rate (mm/rev.)	Depth of Cut (mm)	Ra (μm)	Force (kgf)
1	75	0.8	0.04	1.5	1.01	22.45	31	75	0.4	0.04	1.5	1.09	22.56
2	75	0.8	0.04	1	1.06	15.52	32	75	0.4	0.04	1	1.21	15.16
3	75	0.8	0.04	0.5	1.26	7.67	33	75	0.4	0.04	0.5	1.5	6.62
4	75	0.8	0.06	1.5	1.24	33.21	34	75	0.4	0.06	1.5	1.12	31.44
5	75	0.8	0.06	1	1.32	23.15	35	75	0.4	0.06	1	1.32	21.19
6	75	0.8	0.06	0.5	1.35	11.7	36	75	0.4	0.06	0.5	1.64	9.71
7	75	0.8	0.08	1.5	1.42	39.85	37	75	0.4	0.08	1.5	1.15	38.82
8	75	0.8	0.08	1	1.5	28.07	38	75	0.4	0.08	1	1.4	27.5
9	75	0.8	0.08	0.5	1.61	13.58	39	75	0.4	0.08	0.5	1.93	12.64
10	75	0.8	0.1	1.5	1.6	45.42	40	75	0.4	0.1	1.5	1.28	45.55
11	75	0.8	0.1	1	1.64	32.82	41	75	0.4	0.1	1	1.56	31.73
12	75	0.8	0.1	0.5	1.75	16.94	42	75	0.4	0.1	0.5	2.08	15.48
13	75	0.8	0.12	1.5	1.7	52.26	43	75	0.4	0.12	1.5	1.47	52.8
14	75	0.8	0.12	1	1.78	37.25	44	75	0.4	0.12	1	1.82	37.14
15	75	0.8	0.12	0.5	1.88	19.15	45	75	0.4	0.12	0.5	2.32	17.57
16	90	0.8	0.04	1.5	1.29	20.72	46	90	0.4	0.04	1.5	2.07	22.78
17	90	0.8	0.04	1	1.37	14.14	47	90	0.4	0.04	1	1.42	14.56
18	90	0.8	0.04	0.5	1.4	7.81	48	90	0.4	0.04	0.5	1.75	6.87
19	90	0.8	0.06	1.5	1.41	31.38	49	90	0.4	0.06	1.5	2.22	30.81
20	90	0.8	0.06	1	1.5	21.45	50	90	0.4	0.06	1	1.5	20.5
21	90	0.8	0.06	0.5	1.56	10.66	51	90	0.4	0.06	0.5	1.88	10.2
22	90	0.8	0.08	1.5	1.67	39.14	52	90	0.4	0.08	1.5	2.31	39.8
23	90	0.8	0.08	1	1.72	28.21	53	90	0.4	0.08	1	1.67	27.48
24	90	0.8	0.08	0.5	1.8	14.74	54	90	0.4	0.08	0.5	2.15	13.44
25	90	0.8	0.1	1.5	1.78	44.22	55	90	0.4	0.1	1.5	2.52	46.15
26	90	0.8	0.1	1	1.82	31.56	56	90	0.4	0.1	1	1.82	31.88
27	90	0.8	0.1	0.5	1.93	16.52	57	90	0.4	0.1	0.5	2.28	16.25
28	90	0.8	0.12	1.5	1.93	50.61	58	90	0.4	0.12	1.5	2.9	51.12
29	90	0.8	0.12	1	2.02	36.72	59	90	0.4	0.12	1	2.07	36.57
30	90	0.8	0.12	0.5	2.16	19.46	60	90	0.4	0.12	0.5	2.52	18.7

2.1.1. METHODOLOGY

This study uses a multi-objective optimization approach for ML models. The optimal machining parameters of the NSGA-II algorithm are determined by integrating it with five predictive modeling approaches (SVR, CAT, RFR, GRB, and ANN), and the best model is then selected. It may concurrently reduce tool wear and Ra in the occupied space. Wet machining processing factors such as table feed, cutting speed, depth of cut, and cutting length were taken into consideration as input parameters.

Predictive modelling and NSGA-II are combined in the flowchart in Fig. 1. This flowchart describes the five predictive modelling methods – SVR, CAT, RFR, GRB, and ANN – used to estimate Ra and cutting force: experimental data gathering, dataset extraction, feature selection, and data normalization. The figure also demonstrates how to use GridSearchCV fine-tune to discover the ideal hyperparameter. The best model is then used to forecast Ra and cutting force based on an estimate of the RMSE for the testing dataset. Then, using constraints and the lowest Ra and cutting force, the optimal solutions are discovered in the Pareto front. The final conclusions and observations are presented in Section 4.

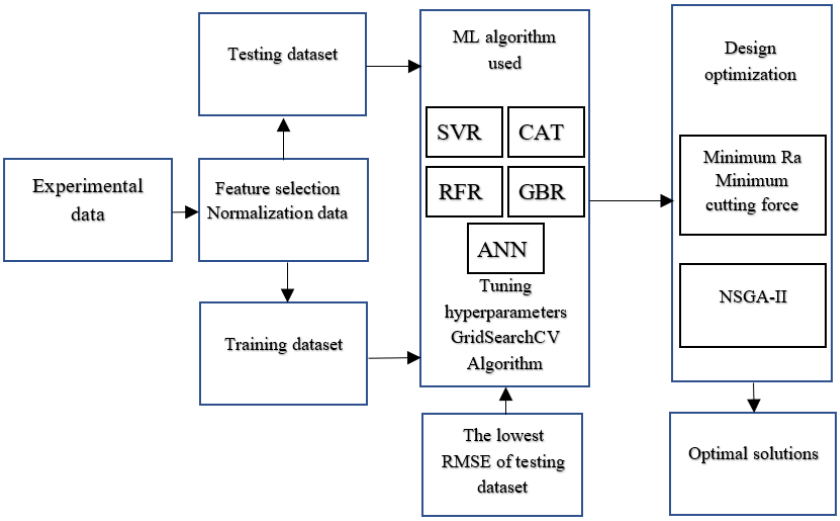

Fig. 1. Combination of ML model and NSGA-II for modelling and optimization in AISI 4340 turning flowchart

Feature extraction, a crucial step in machine learning, involves turning raw data gathered from numerous signal channels into a set of statistical features in a manner that is compatible with machine-learning algorithms. A machine-learning algorithm is then given the statistical information as input. The experiment utilized four input parameters, which included cutting speed, nose radius, feed rate, and depth of cut. Besides, surface roughness and cutting force were selected as the output parameters and measured from the experiment. These two output parameters characterize the machining process's quality and energy cost.

LIN, SVR, GBR, and ANN were each used to create one of four predictive models. For the purpose of developing the model, two-thirds (2/3) of the input data were randomly chosen (training). The remaining 1/3 of the input data was used to validate the model (testing).

3. MACHINE LEARNING TECHNIQUES AND OPTIMIZATION PROCEDURES

3.1. MACHINE LEARNING TECHNIQUES

1. SVM regression

Support Vector Machine (SVM) is a classic machine-learning algorithm that can be used for classification and regression problems. The principle of SVM was first introduced by Vapnik et al. [28]. SVM can be used to solve linear and nonlinear problems by separating

the database into classes using an ideal hyperplane (see Fig. 2). The hyperplane is considered ideal when the distance between 2 data classes is maximized.

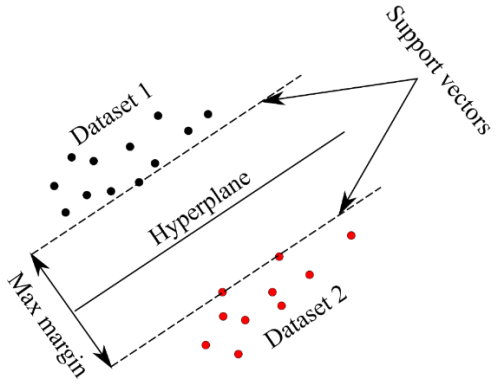

Fig. 2. Illustration of Support Vector Machine algorithm

In terms of advantages, SVM can be very effective in high dimensional spaces, which suits the problems when the input data is composed of several variables. SVM is also efficient in terms of memory, as it only uses a subset of training data in the decision function. Finally, SVM is quite versatile, as several functions can be used for the decision function.

In terms of limitations, overfitting can be a major problem when the number of features in the input data is much higher than the number of considered samples. In this case, serious regulation processes are needed to avoid overfitting.

2. Categorical Gradient Boosting (CAT)

Decision trees are used as the primary predictors in the majority of gradient-boosting implementations. Decision trees are useful for numerical features, but in reality, many datasets contain categorical features that are essential for prediction. Yandex created the unique gradient-boosting technology known as CAT. Within the gradient-boosting tree algorithmic framework, it is a better implementation. A symmetrical decision tree algorithmic method with few parameters, support for categorical variables, and excellent accuracy is the foundation of this system [29]. The algorithm's accuracy and generalizability are enhanced by CAT [30]. It has been successfully used in a variety of fields, including biomass, evapotranspiration, media popularity prediction, and weather forecasting [31–32]. This is the reason the model is used here to forecast how well ultra-precision machining will work.

3. Decision-Tree Regression (DTR)

Traditional ML techniques include decision trees (for classification and regression). Overall, their learning capabilities are not excellent, but they are renowned for their generalizability and feature filtering. They are known as regression trees when applied to regression tasks [33]. The model continues to pick up new information as the number of iterations rises. Hyperparameters like the number of features that are selected, the maximum depth of the tree, and the minimum sample size of branches can truncate the training process.

4. Gradient-Boosted Trees

Gradient-Boosted Trees (GBT) is a machine-learning technique based on an ensemble of weak prediction models [34]. The main principle of Gradient-Boosted Trees is that each

model in the ensemble tries to predict the error left over by the previous model. GBT can be used for both regression and classification problems.

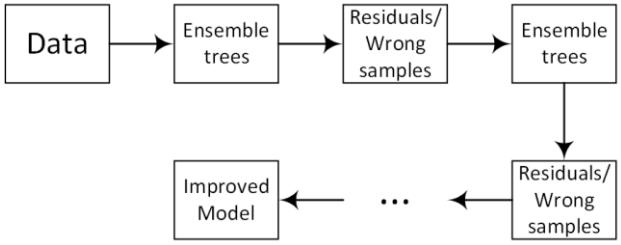

Fig. 3. Flowchart of Gradient Boosted Trees algorithm

As described in Fig. 3, the weak predictive models are fitted into the model so each new leaner fit into the residuals of the previous step so that the model improves. The final improved model aggregates the results of each step and becomes a strong predictive model.

5. ANN regression

Artificial Neural Network (ANN) machine-learning models are inspired by the functions of human brains [35]. The main component of ANN is artificial neurons or nodes. Each ANN structure is composed of several layers, and each layer is a group of neurons acting at the same level. These neurons are interconnected between each layer but the neurons in the same layer are not connected. The minimum number of layers in an ANN structure is 3:

- Input layer that contains input variables and passes them to the next layer.
- Hidden layer that contains node functions for training the model.
- Output layer that receives the results from the previous hidden layer and exports the output.

One ANN structure can contain one or several hidden layers, depending on the objective of the problem. When the number of hidden layers is greater than one, the model is called a deep neural network. A typical architecture of ANN is shown in Fig. 4.

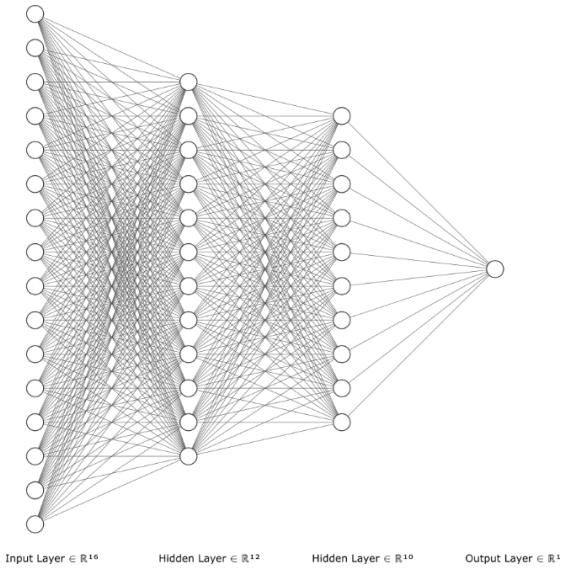

Fig. 4. Architecture of ANN model

One of the main advantages of ANN is its ability to work with any type of input data [36–37] Another advantage of ANN is the capability of parallel computing, which can be highly beneficial when dealing with large datasets. On the other hand, ANN's limitations need to be considered, such as the high memory cost, as the information is stored on the entire network. In addition, several trials need to be carried out to find the optimal number of layers, as the behaviour of ANN is hard to control.

6. Performance evaluation

Building an effective machine-learning model requires evaluation. Only a few assessment metrics can be utilized for regression, out of the many evaluation metrics available. RMSE, MAE, and R^2 are the assessment metrics most often used in the regression. These metrics' formulas are as follows:

$$RMSE = \sqrt{\frac{\sum_{i=1}^{N}(\hat{y}_i - y_i)^2}{N}}$$
$$MAE = \frac{1}{N}\sum_{i=1}^{N}|\hat{y}_i - y_i| \tag{1}$$
$$R^2 = 1 - \frac{\sum_{i=1}^{N}(\hat{y}_i - y_i)^2}{\sum_{i=1}^{N}(\hat{y}_i - \overline{y})^2}$$

where the actual and forecast values are denoted by yi and $\hat{y}_i$, respectively. The overall number of observations is N. Higher R^2 values and lower RMSE and MAE values indicate a more accurate model. RMSE has an advantage over MAE in that it does not use absolute value, which is a highly undesirable method in many mathematical calculations [38]. Because RMSE is easier to compute and distinguish between, it is a superior choice when evaluating the predicted accuracy of various regression models. It is preferable for R^2 to be higher [39].

3.2. MULTI-OBJECTIVE OPTIMIZATION

NSGA-II is a multi-objective algorithm used widely to solve engineering problems [14], [21–22] Launched by Deb [40], NSGA-II still has a great value. The genetic algorithm's mating and survival selection were modified to create the algorithm. Generally speaking, NSGA-II picks out, hybridizes, mutates, and ranks non-dominant solutions to guarantee strong Pareto front convergence and do away with local optimization. The mathematical-style pseudocode of NSGA-II is shown in Fig. 5.

It is necessary, during the manufacturing process, to find the best way to decrease material, labor, energy, time, cutting tool, and financial waste, in order to minimize fabrication costs. Therefore, it is necessary to improve the cutting parameters. The two criteria minimum Ra and minimal cutting force must be satisfied at the same time. NSGA-II is used to find Pareto-optimal methods to solve this problem.

Material removal rate and basic cutting parameters have a direct impact on cutting power and cutting forces (i.e., cutting speed, feed rate, and depth of cut). Reduced machining time

is one of the goals of optimizing the machining process. One method is to increase the material removal rate, i.e., the cutting parameters.

NSGA-II procedure

Input: N, T, $\mathcal{F}_k(X) \triangleright N$ members evolved T generations to solve Min $f_k(X)$
Initialize Population P_0 size N randomly;
for $t = 1$ to T do
  Generate next offspring population Q_t size N by:
    Binary Tournament Selection;
    Crossover and Mutation;
  Combine current Parents P_t and new Offspring Q_t to form R_t;
  Calculate objective values for R_t;
  Assign Rank (level) for R_t based on Pareto fronts $\mathcal{F}_k$ (non-dominated solutions);
  Calculate Crowding distance (CD) for each solution in R_t;
  Initialize next Parent population P_{t+1} by the following loop:
  Add solutions in lowest rank Pareto fronts with priority for a greater CD until N individuals are obtained;
end
end

Fig. 5. Pseudocode of NSGA-II [41]

This, however, results in increased cutting force and lower surface quality. As a result, selecting cutting parameters to achieve criteria such as good surface quality, quick machining time, and low energy consumption is fraught with uncertainty. To solve this problem, the best combination of parameters for improving machining performance must be determined. As a result, optimizing cutting force and surface roughness is critical for long-term production, which includes energy consumption, machining costs, product quality, and environmentally friendly manufacturing.

4. RESULTS AND DISCUSSION

4.1. HYPERPARAMETER TUNING WITH GRIDSEARCHCV

This work uses the GridSearchCV [42] package to determine the hyperparameter for the ML model. The predefined values for hyperparameter in the GridSearchCV function are shown in Table 2. The LIN model has no hyperparameters. Meanwhile, SVR, GBR, and ANN models have many hyperparameters, which control the overfitting and underfitting of the model. Therefore, an apt hyperparameter choice can lessen overfitting and improve the predictive precision. A large number of initial hyperparameters for SVR, GRB, and ANN are shown in Table 3, which have to be examined in order to identify the most suitable optimum values. In order to save computing time, hyperparameters are chosen in this work by a computer, concentrating on important and valuable parameter effects on the performance of the ML model.

For SVR, GRB, and ANN, the hyperparameter values utilized are kernel, *C*, degree, and gamma; for CAT, RFR, GBR, and RFR, the variables are depth, interaction, bootstrap, *n*

estimators, learning rate, max depth, and subsample; and for ANN, the values are batch size, epochs, optimizer, and hidden layers. In addition, the accuracy metrics of RMSE are employed as criteria to determine optimal parameter values.

Table 3. Hyperparameters for machine learning models

Algorithm	Hyperparameters Tuned	Predictive Ra (Ra)		Cutting force	
		Grid space	Results	Grid space	Results
SVR	kernel	[‘rbf’, ‘sigmoid’]	'rbf'	['rbf', 'sigmoid', 'poly']	'rbf'
	C	[450, 500, 550, 600]	550	[12, 15, 18, 20]	15
	degree	[0, 1e-6, 2e-6, 1e-5, 1e-4]	0	[0, 1e-6, 2e-6, 1e-5, 1e-4]	0
	gamma	[5e-3, 8e-3, .01, .02, .05, .1]	8e-3	[0.04, .045, 0.05, .055, 0.6]	0.055
CAT	depth	[3, 4, 6]	4	[3, 4, 6]	3
	learning_rate	[0.01, 0.05, 0.1, .12, .15, .2]	0.1	[0.01, 0.05, 0.1, .12, .15, .2]	0.05
	iterations	[50, 100, 200, 300]	300	[50, 100, 200, 300]	300
RFR	n_estimators	[400, 500, 600]	500	[400, 500, 600]	600
	max_features	['auto', 'sqrt', 'log2']	Auto	['auto', 'sqrt', 'log2']	sqrt
	min_samples_split	[1,2,4]	2	[1,2,4]	2
	bootstrap	[True, False]	True	[True, False]	False
GBR	n_estimators	[100, 500, 1000, 1500]	500	[100, 500, 1000, 1500]	500
	learning_rate	[0.01, 0.02, 0.02, 0.04]	0.02	[0.01, 0.02, 0.02, 0.04]	0.04
	max_depth	[4, 6, 8, 10]	6	[6, 8, 10, 12]	10
	subsample	[0.1, 0.2, 0.5, 0.9]	0.2	[0.1, 0.2, 0.5, 0.9]	0.2
ANN	batch_size	[140, 200, 250]	200	[10, 12, 15, 20]	15
	epochs	[200, 300, 350]	350	[250, 300]	300
	optimizer	['adam', 'rmsprop']	'adam'	['adam', 'rmsprop']	'adam'
	units1	[100, 80]	100	[80, 64]	64
	units2	[36, 28]	36	[50, 45]	48
	units3	[16, 10]	16	[10, 8]	10

4.2. HYPERPARAMETER TUNING WITH GRIDSEARCHCV

4.2.1. PREDICTION CAPABILITY FOR Ra

In the present study, five ML models – namely SVR, CAT, RFR, GBR, and ANN – have been used to predict surface roughness. To assess the predictive performance of these ML models, three accuracy errors, MAE, RMSE, and R^2, have been employed on the statistics in Table 4 on the training and testing datasets. With the training dataset, CAT achieves the best accuracy in predicting the Ra values with RMSE of 0.0626, MAE of 0.0482, and the highest R^2 of 0.9791. However, CAT seems to have poorer predictive performance on the

testing dataset with an R^2 of 0.7332. Meanwhile, ANN was the best-performing of the five ML models on both the training and testing datasets. Indeed, while the RMSE value of the ANN model tested is 0.1095, the corresponding RMSE values for the SVR, CAT, RFR, and GBR are 0.2038, 0.1808, 0.2011, and 0.1959, respectively. In addition, the predictive performance of the ANN exhibits the lowest MAE = 0.0947 and the highest R^2 = 0.8996. Besides, ANN also demonstrates good predictive ability on the training dataset with an R^2 of 0.9557. Moreover, the high value of R^2 indicated that the predicted values closely match the measured experimental values. Therefore, ANN outperforms the rest of the models.

Figures 6 and 7 offer a graphical comparison between the measured experimental values and the values predicted by SVR, CAT, RFR, GBR, and ANN on the training and testing datasets. The different colors of the line and scatter reflect the values predicted by other ML models and measured values. In these figures, the superior prediction performance of ANN can be noted by the close match of each data point on the graph with the measured values of Ra. Indeed, the proximity of the values predicted by ANN and the measured value is confirmed by the lowest values of RMSE and MAE and the highest value of the coefficient of determination. Besides, some values of results predicted by SVR, RFR, and GBR do not conform closely to the Ra value found experimentally. In summary, ANN is the most reliable model in predicting Ra, and for that reason, it is selected for the following procedure.

Table 4. Statistical accuracy metrics of ML models for Ra prediction on the training and testing datasets

Accuracy metric	SVR	CAT	RFR	GBR	ANN	Data
MAE	0.1402	0.0482	0.0644	0.0614	0.0717	Training dataset
RMSE	0.1726	0.0626	0.0919	0.0878	0.0974	
R^2	0.8378	0.9791	0.9635	0.9595	0.9577	
MAE	0.1732	0.1454	0.1625	0.1482	0.0947	Testing dataset
RMSE	0.2308	0.1808	0.2011	0.1959	0.1095	
R^2	0.6642	0.7332	0.6603	0.6581	0.8996	

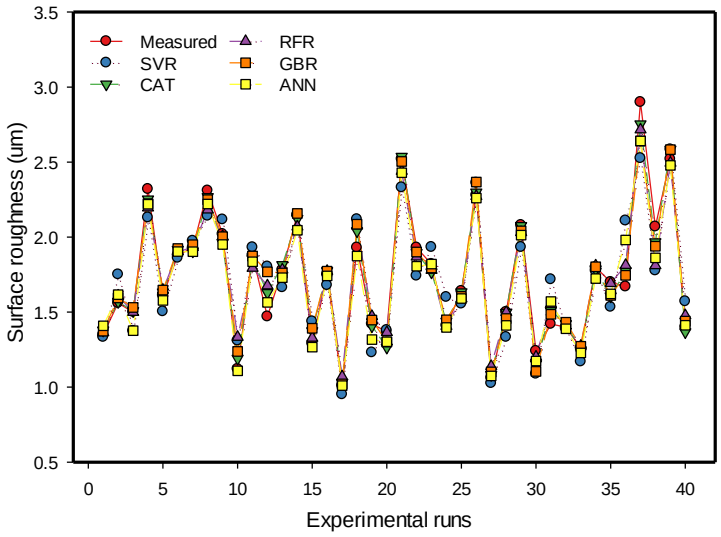

Fig. 6. Ra experimental measurement and predicted values on the training dataset

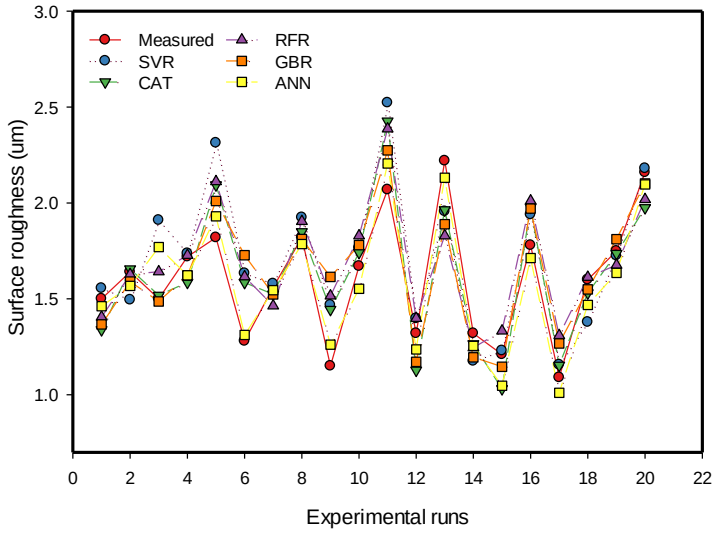

Fig. 7. Ra experimental measurement and prediction values on the testing dataset

4.2.2. PREDICTION CAPABILITY FOR CUTTING FORCE

Similarly, five ML models – SVR, CAT, RFR, GBR, and ANN – also predict cutting force. The statistical accuracy metrics of various models for predicting V.B. based on the training and testing datasets are summarized in Table 5. RFR exhibits the best predictive performance on the training dataset, with RMSE and MAE of zero and R^2 of 1. However, RFR performs terribly in predicting the cutting force values on the testing dataset, with RMSE of 2.0976 and MAE of 1.6812; these values are poorer than the RMSE and MAE values delivered by CAT, GBR, and ANN, as shown in Table 5. ANN exhibits the best predictive performance on the testing dataset out of the five models. Indeed, while the RMSE value of the ANN model is 0.7477, the corresponding RMSE values for SVR, CAT, RFR, and GBR are 2.5896, 0.7832, 2.0976, and 0.8024, respectively.

Moreover, ANN exhibits the lowest MAE = 0.6442 and a high R^2 value. Besides, the high value of R^2 of 0.9988 (training) and 0.9950 (testing) indicated that the predicted values closely match the measured experimental values. Therefore, the ANN outperforms the rest of the models in terms of all accuracy metrics. The predicted and measured results in terms of cutting force are presented by the line and scatter plot for the training and testing datasets, in Fig. 8 and Fig. 9, respectively. The colors in these figures reflect the values predicted by different ML models.

Table 5. Statistical accuracy metrics of ML models for cutting force prediction on the training and testing datasets

Accuracy metric	SVR	CAT	RFR	GBR	ANN	Data
MAE	2.3517	0.1733	0.0000	0.2389	0.3830	Training dataset
RMSE	2.7639	0.2067	0.0000	0.3082	0.4808	
R^2	0.9640	0.9998	1.0000	0.9995	0.9988	
MAE	2.2300	0.6691	1.6812	0.6443	0.6442	Testing dataset
RMSE	2.5896	0.7832	2.0976	0.8024	0.7477	
R^2	0.9547	0.9958	0.9958	0.9950	0.9950	

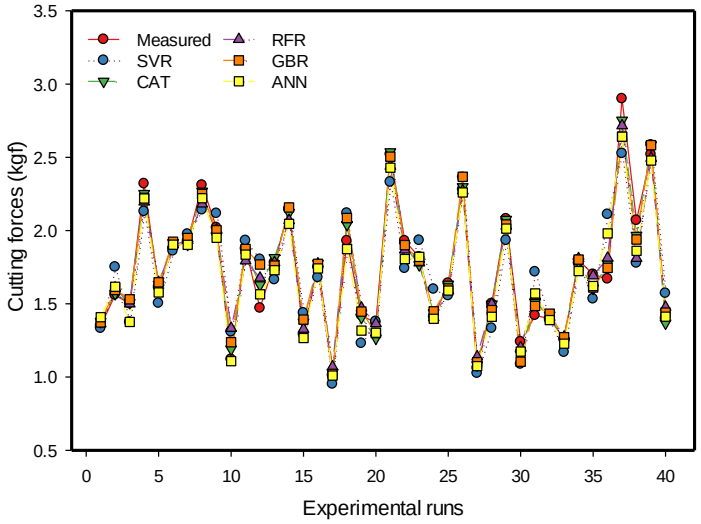

Fig. 8. Experimental measurement values and cutting force predictions on the training dataset

In terms of the training dataset (in Fig. 8), the values predicted by CAT, RFR, GBR, and ANN are close to the cutting force measured experimentally. In terms of the testing dataset, ANN's predicted values are nearest to the measured cutting force. Indeed, the proximity of the values predicted by these models and the measured value are confirmed by the lowest RMSE and MAE values and the highest value of R^2. In summary, ANN is the most reliable model in predicting cutting force and is selected for the following procedure.

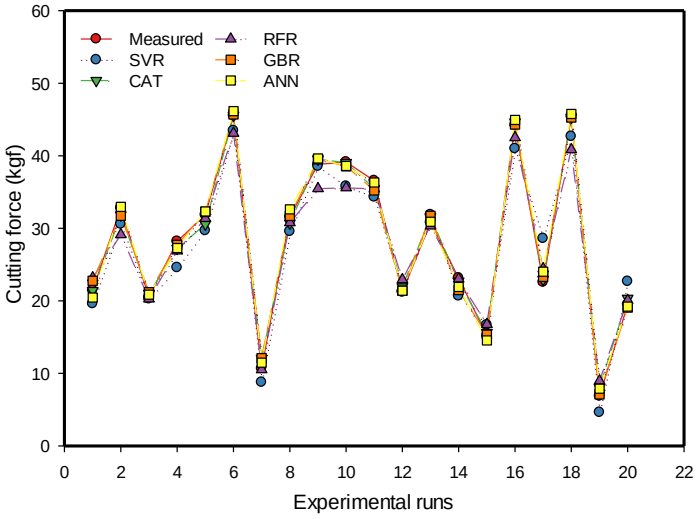

Fig. 9. Experimental measurement values and cutting force predictions on the testing dataset

4.3. MULTI-OBJECTIVE OPTIMIZATION BY NSGA-II

This work aims to find reasonable turning parameters that minimize the surface roughness and cutting force. However, these objective functions conflict with one another, so multi-objective optimization is the best choice to solve this problem. As discussed in Section

4.2, the ANN model exhibits the best predictive performance with respect to Ra and cutting force. Therefore, the formulation that defines the multi-objective problem can be written as Equation 2, where ANN_reg_Ra and ANN_reg_force are models predicting Ra and cutting force, respectively. These models take different hyperparameters, as selected in Table 6, into account.

For the constraint boundary, ranges of values of machining parameters have been used to define the lower and upper variable bounds of cutting speed, feed rate, depth of cut, and tool nose radius. Recent literature [23], [25–27], [43–44] suggests the range of process parameters in the turning AISI 4340 steel, presented in Table 1. Therefore, this study chooses a range of cutting speed, feed rate, depth of cut, and tool nose radius of, respectively, 50–375 m/min, 0.02–0.25 mm/rev, 0.1–1.5 mm, and 0.4–0.8 mm. All constraint boundaries have been normalized corresponding to each ML model. Analytically, the Pareto front solutions are given by: $PS = \{(V_c, f, a, r) | (50 \leq V_c \leq 375) \wedge (0.02 \leq f \leq 0.25) \wedge (0.1 \leq a \leq 1.5) \wedge (0.4 \leq r \leq 0.8)\}$. These constraint boundaries are written in Equation 3.

Table 6. Statistics of process parameters in turning AISI 4340 steel

No.	Literature	Cutting speed (m/min)	Feed rate (mm/rev)	Depth of cut (mm)	Nose radius (mm)
1	Çydaş et al [23]	60–90	0.08–0.24	0.1–0.3	0.8
2	Das et al. [27]	100–220	0.05–0.13	0.2–0.6	0.8
3	Gupta et al. [26]	51–141	0.197–0.248	1.0	0.4
4	Rashid et al. [43]	90–250	0.02–0.15	0.1–0.4	0.8
5	Dennison et al. [44]	325–375	0.1–0.2	0.3–0.9	0.4
6	Patole et al. [25]	75–90	0.04–0.12	0.05–0.15	0.4–0.8

Objectives

$$\begin{aligned} \text{Minimize Ra} &= \text{ANN\_}r\text{eg\_Ra}(V_c, f, a, r) \\ \text{Minimize cutting force} &= \text{ANN\_reg\_force}(V_c, f, a, r) \end{aligned} \tag{2}$$

Subject to constraints

$$\begin{aligned} 50 \leq V_c \leq 375 \\ 0.02 \leq f \leq 0.25 \\ 0.1 \leq a \leq 1.5 \\ 0.4 \leq r \leq 0.8 \end{aligned} \tag{3}$$

Surface roughness and cutting force must be as low as possible in machining. Hence, the NSGA-II algorithm implemented in the Python environment has been used to find the optimal machining parameters for manufacturing. In the operating of the algorithm, the initial parameter settings were: population size of 50, maximum generation of 100, crossover rate of 0.85, mutation rate of 0.2, and selection rate of 0.25, as shown in Table 7.

Table 7. Parameters for NSGA-II

Input parameter	Population size	Maximum generations	Crossover rate	Mutation Rate	Selection rate
Value	50	100	0.85	0.2	0.25

The NSGA-II algorithm appears to converge successfully after 2500 simulation runs. Fifty optimal solutions lie on the Pareto front, evenly distributed and representative, as shown in Fig. 10. Pareto solutions are marked in red. The first performance objective – i.e., Ra – was found to lie between 1.014 and 1.057 μm. The second performance objective – i.e., cutting force – was found to range between 7.793 and 19.007 kgf for the fifty Pareto solutions. However, according to ISO 883:2013, the tool nose radius is standardized with values of 0.2, 0.4, 0.8, 1.2 mm, and so on. Therefore, five solutions were selected and highlighted as black rectangles in Fig 10 (with a nose radius of 0.4 mm). On the other hand, the surface roughness lies between 1.032 and 1.048 μm, and cutting force was found to range between 7.981 and 8.277 kgf.

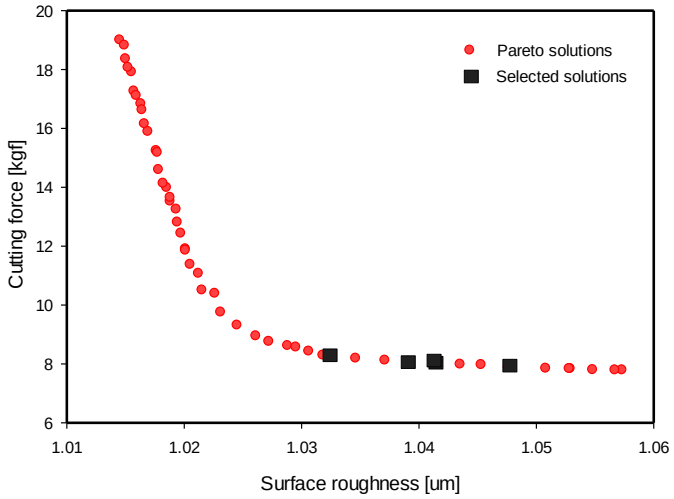

Fig. 10. Performance statistics obtained for 50 Pareto solutions

Table 8. Result of Pareto solutions generated by multi-objective NSGA-II

Solutions	*Vc*	Feed rate	Depth of cut	Tool nose radius	Surface roughness	Cutting force
1	78.34	0.02	1.50	0.75	1.015	19.007
2	71.23	0.02	0.53	0.42	1.057	7.793
3	**72.92**	**0.02**	**0.62**	**0.40**	**1.048**	**7.891**
4	74.64	0.02	0.76	0.41	1.035	8.189
5	72.58	0.02	0.60	0.42	1.051	7.852
6	74.47	0.02	0.86	0.51	1.026	8.949
7	76.77	0.02	1.25	0.67	1.018	14.601
8	72.91	0.02	0.65	0.41	1.045	7.973
9	78.23	0.02	1.35	0.62	1.017	15.900
10	74.67	0.02	1.01	0.52	1.023	10.394
11	76.07	0.02	1.06	0.53	1.021	11.072
12	72.92	0.02	0.65	0.45	1.044	7.987
13	76.10	0.02	1.13	0.61	1.020	12.440
14	76.07	0.02	1.06	0.57	1.021	11.380
15	71.05	0.02	0.55	0.44	1.055	7.804
16	75.85	0.02	1.00	0.55	1.022	10.507
17	74.64	0.02	0.84	0.50	1.027	8.763
18	74.46	0.02	0.93	0.57	1.023	9.759
19	74.46	0.02	0.91	0.51	1.025	9.315
20	78.58	0.02	1.46	0.66	1.016	17.924
21	76.60	0.02	1.29	0.67	1.018	15.245
22	74.67	0.02	0.81	0.43	1.031	8.430
23	78.15	0.02	1.36	0.64	1.017	16.157

24	**75.11**	**0.02**	**0.79**	**0.40**	**1.032**	**8.277**
25	74.28	0.02	0.72	0.42	1.037	8.122
26	78.64	0.02	1.48	0.69	1.015	18.365
27	74.67	0.02	0.84	0.45	1.029	8.619
28	78.64	0.02	1.50	0.69	1.015	18.827
29	**74.07**	**0.02**	**0.71**	**0.40**	**1.039**	**8.082**
30	78.14	0.02	1.41	0.69	1.016	17.268
31	76.60	0.02	1.29	0.67	1.018	15.182
32	76.38	0.02	1.10	0.59	1.020	11.904
33	76.83	0.02	1.19	0.57	1.019	13.257
34	**73.21**	**0.02**	**0.71**	**0.40**	**1.041**	**8.072**
35	74.64	0.02	0.84	0.44	1.030	8.569
36	71.20	0.02	0.53	0.42	1.057	7.796
37	76.81	0.02	1.16	0.57	1.019	12.818
38	76.31	0.02	1.10	0.58	1.020	11.857
39	78.14	0.02	1.38	0.71	1.016	16.839
40	**73.21**	**0.02**	**0.71**	**0.40**	**1.041**	**8.074**
41	76.60	0.02	1.23	0.63	1.019	13.994
42	78.14	0.02	1.40	0.69	1.016	17.117
43	76.60	0.02	1.23	0.66	1.018	14.140
44	75.11	0.02	0.79	0.42	1.032	8.293
45	72.58	0.02	0.59	0.42	1.053	7.838
46	78.64	0.02	1.46	0.69	1.015	18.076
47	72.58	0.02	0.59	0.41	1.053	7.839
48	78.00	0.02	1.37	0.70	1.016	16.628
49	76.60	0.02	1.20	0.63	1.019	13.529
50	76.60	0.02	1.20	0.66	1.019	13.657

Table 8 lists the 50 solutions that make up the Pareto-optimal solution set, along with the tuning parameter that goes with each one, which consists of five suitable solutions in reality that are bold-highlighted. Table 9 summarizes the selected Pareto solution's range of values generated by NSGA-II. As a result, cutting speeds between 72.92 and 75.11 m/min, a feed rate of 0.02 mm/rev, a depth of cut between 0.62 and 0.79 mm, and a tool nose radius of 0.4 mm, are recommended. Whereby, selected Pareto solutions indicated that surface roughness lies between 1.032 and 1.048 μm, and cutting force was found to range between 7.891 and 8.277 kgf.

Table 9. Selected Pareto solutions produced by the multi-objective NSGA-II have a wide range of values

Range	Cutting speed	Feed rate	Depth of cut	Tool nose radius	Ra	Cutting force
	(m/min)	(mm/rev)	(mm)	(mm)	(μm)	(kgf)
Minimum	72.92	0.02	0.62	0.4	1.032	7.891
Maximum	75.11	0.02	0.79	0.4	1.048	8.277

5. VALIDATION OF THE OPTIMAL RESULTS

In this section, experiments were performed to confirm the five selected Pareto solution results. According to Table 8, cutting parameters were taken from solutions 3, 24, 29, 34, and 40 (Bold highlighted). In addition, turning tests were carried out on the FEL-1440GMW MAGNUM-CUT lathe based on these configurations. All experiments were conducted under

the MQL with a flow rate of Ethylene Glycol coolant of 140 ml/hr. The tungsten carbide indexable inserts CCMT-090304 had a 0.4 mm nose radius—the tool holder of grade K10.

Cylindrical AISI 4340 specimens, 24 mm diameter and 100 mm length, were used as workpieces. Specialized jig clamped a dynamometer Kistler Type 9139AA, which was mounted in a tool holder. The detail of the experiment is illustrated in Fig. 11.

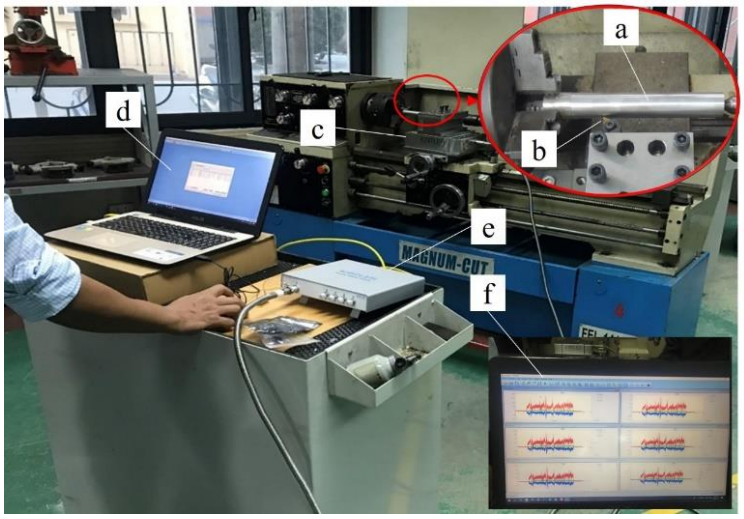

Fig. 11. Experimental system: a) Workpiece, b) Cutting insert, c) Dynamometer, d) DynoWare software, e) Data processing box, f) Cutting force results

The studies measured cutting force elements in all three directions (X direction: F_x, Y direction: F_y, and Z direction: F_z) were measured in the experiments as shown in the schematic arrangement in Fig. 12. A three-components turning dynamometer was employed for recording the force values. The resultant cutting force was calculated using the following formula:

$$F = \sqrt{F_x^2 + F_y^2 + F_z^2} \tag{4}$$

Besides, the surface roughness was measured three times along the machined part axis by a Mitutoyo-Surftest SJ-210 Portable, and the average of them was taken as the final value. All measurement results are presented in Table 10.

As shown in Table 10, the test results are close to the predicted values obtained from NSGA-II optimization. Regarding the absolute percentage errors (APE), Ra and cutting force exhibit the largest values of APE (12.67% and 6.33%, respectively). Meanwhile, the values of mean absolute percentage errors (MAPE) are 9.41% and 3.55% for Ra and cutting force, respectively. From these results, it can be seen that the MAPE metrics of surface roughness are quite large. It might be due to the following reasons: experimental procedures, machining machines, and measuring equipment installations. However, the test results also partly proved that NSGA-II and ML might be combined together in turning operations to optimize the Ra and cutting force.

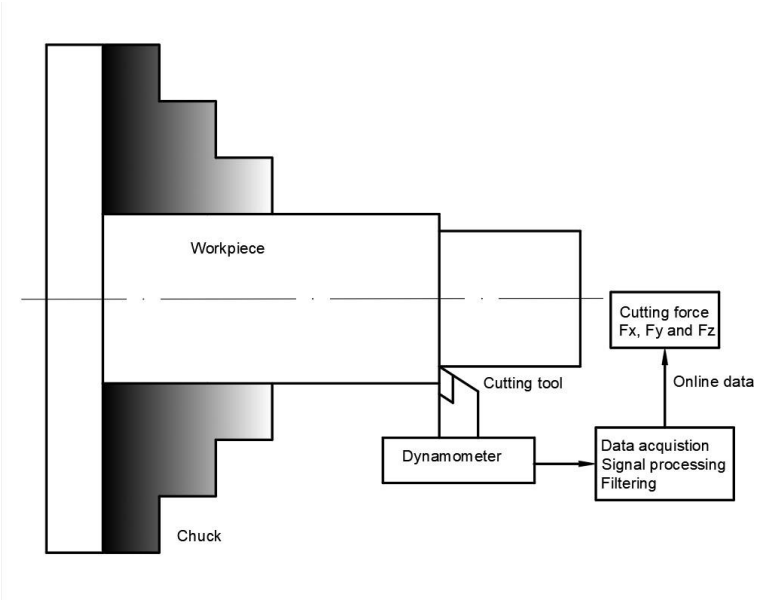

Fig. 12. Schematic layout of cutting force measurement setup

Table 10. Validation of predicted results

No.	Cutting speed (m/min)	Feed rate (mm/rev.)	Depth of cut (mm)	Tool nose radius (mm)	Optimal results		Experimental results		Absolute percentage error	
					Ra (μm)	Cutting force (kgf)	Ra (μm)	Cutting force (kgf)	Ra (μm)	Cutting force (kgf)
1	72.92	0.02	0.62	0.4	1.048	7.891	1.112	8.135	5.76%	4.18%
2	75.11	0.02	0.79	0.4	1.032	8.277	0.954	8.436	8.18%	6.33%
3	74.07	0.02	0.71	0.4	1.039	8.082	1.139	8.562	8.78%	5.61%
4	73.21	0.02	0.71	0.4	1.041	8.072	0.932	7.987	1.70%	1.06%
5	73.21	0.02	0.71	0.4	1.041	8.074	1.214	8.026	12.67%	0.60%
Mean Absolute Percentage Errors									9.41%	3.55%

6. CONCLUSION

This study discusses the hybridization of machine learning and NSGA-II in multi-objective optimization. The objective functions are a simultaneous minimum of surface roughness and cutting force for turning AISI 4340 steel. The turning parameters, such as surface roughness and cutting force, are compared with predictive results by five ML models: SVR, CAT, RFR, GBR, and ANN. By all accuracy metrics, ANN is the best-performing model in predicting surface roughness and cutting force on the training and testing datasets.

Surface roughness and cutting force must be as low as possible in machining. Hence, the NSGA-II algorithm implemented in Python has been used to find the optimal machining parameters for manufacturing. Pareto solutions indicated that surface roughness lies between 1.032 and 1.048 μm, and cutting force is found between 7.981 and 8.277 kgf for the five selected Pareto solutions. Results summarize the range of values in the Pareto solution

generated by NSGA-II: cutting speeds between 72.92 and 75.11 m/min, a feed rate of 0.02 mm/rev, a depth of cut between 0.62 and 0.79 mm, and a tool nose radius of 0.4 mm, are recommended. The values of MAPE of Ra and cutting force were 9.41% and 3.55%, respectively, according to the experimental verification results.

Thus, this study proved that the multi-objective optimization strategy performed well within an accepted range of errors for Ra and cutting force. The raw/processed data required to reproduce these findings will be made available on request. Nonetheless, further research is required to create an intelligent system that uses NSGA-II as a decision-making tool to incorporate user preferences. In addition, future research should focus on cutting forces to understand the mechanical process better.

Moreover, general problems of manufacturing costs such as labor, energy, time, cutting tools (geometry, materials, tool wears), waste of materials, and product quality should be performed in the next works. Besides, cutting tool micro characteristics such as edge radius, rake angle, nose radius, vary with tool wear and direction of cutting, thermal conditions, build-up edge, chip type and shape and process stability (vibration) should also be considered.

REFERENCES

[1] ROY S., KUMAR R., DAS R.K., SAHOO A.K., 2018, *A Comprehensive Review on Machinability Aspects in Hard Turning of Aisi 4340 Steel*, In Iop Conference Series: Materials Science and Engineering, 390/1, 012009.

[2] RASHID W.B., GOEL S., LUO X., RITCHIE J.M., 2013, *An Experimental Investigation for the Improvement of Attainable Surface Roughness During Hard Turning Process*, Proc. Inst. Mech. Eng. Part B, J. Eng. Manuf., 227/2, 338–342.

[3] Yi Q., TANG Y., LI C., Li P., 2013, *Optimization Of Cnc Machine Processing Parameters for Low Carbon Manufacturing*, In Ieee International Conference on Automation Science and Engineering (Case), 498–503.

[4] RAO S.N., SATYANARAYANA B., VENKATASUBBAIAH K., 2011, *Experimental Estimation of Tool Wear and Cutting Temperatures in MQL Using Cutting Fluids with CNT Inclusion*, Int. J. Eng. Sci. Technol., 3/4.

[5] ADHEIL H.S., ISMAIL N., 2010, *Optimization of Cutting Parameters of Turning Operations by Using Geometric Programming*, Am J Eng Appl Sci, 102–108.

[6] GUPTA M.K., et al., 2021, *Tribological Performance Based Machinability Investigations in Cryogenic Cooling Assisted Turning of A-B Titanium Alloy*, Tribol. Int., 160, 107032.

[7] BAGAWADE D., RAMDASI P.G., 2014, *Effect of Cutting Parameters on Material Removal Rate and Cutting Power During Hard Turning of Aisi 52100 Steel*, Int. J. Eng. Res. Technol., 3/1.

[8] KUNTOGLU M., et al., 2021, *Parametric Optimization for Cutting Forces and Material Removal Rate in the Turning of AISI 5140*, Machines, 9/5, 90, https://doi.org/10.3390/machines9050090.

[9] PIMENOV D.Y., ABBAS A.T., GUPTA M.K., ERDAKOV I.N., SOLIMAN M.S., El Rayes M.M., 2020, *Investigations of Surface Quality and Energy Consumption Associated with Costs and Material Removal Rate During Face Milling of Aisi 1045 Steel*, Int. J. Adv. Manuf. Technol., 107/7, 3511–3525.

[10] YAN J., LI L., 2013, *Multi-Objective Optimization of Milling Parameters–The Trade-Offs Between Energy, Production Rate and Cutting Quality*, J. Clean. Prod., 52, 462–471.

[11] MARKO H., SIMON K., TOMAZ I., MATEJ P., JOZE B., MIRAN B., 2014, *Turning Parameters Optimization Using Particle Swarm Optimization*, Procedia Eng., 69, 670–677.

[12] D'ADDONA D.M., TETI R., 2013, *Genetic Algorithm-Based Optimization of Cutting Parameters in Turning Processes*, Procedia Cirp, 7, 323–328.

[13] AHSAN HABIB M., PATWARI M., ANAYET U., KHAN K.A., 2015, *Amanullah Tomal A.N.M., Surface Roughness Optimization in Turning Operation Using Hybrid Algorithm of Artificial Bee Colony with Rsm*, Advanced Materials Research, 1101, 393–396.

[14] BOUACHA K., TERRAB A., 2016, *Hard Turning Behavior Improvement Using NSGA-II and PSO-NN Hybrid Model*, Int. J. Adv. Manuf. Technol., 86/9, 3527–3546.

[15] NGUYEN A.-T., NGUYEN V.-H., LE T.-T., NGUYEN N.-T., 2022, *Multiobjective Optimization of Surface Roughness and Tool Wear In High-Speed Milling of AA6061 by Machine Learning and NSGA-II,* Adv. Mater. Sci. Eng., https://doi.org/10.1155/2022/5406570.
[16] KAO Y.-T. ZAHARA E., 2008, *A Hybrid Genetic Algorithm and Particle Swarm Optimization for Multimodal Functions,* Appl. Soft Comput., 8/2, 849–857.
[17] SARDINAS R.Q., SANTANA M.R., BRINDIS E.A., 2006, *Genetic Algorithm-Based Multi-Objective Optimization of Cutting Parameters in Turning Processes,* Eng. Appl. Artif. Intell., 19/2, 127–133.
[18] CHUANGWEN X., JIANMING D., YUZHEN C., HUAIYUAN L., ZHICHENG S., JING X., 2018, *The Relationships Between Cutting Parameters, Tool Wear, Cutting Force and Vibration,* Adv. Mech. Eng., 10/1, https://doi.org/10.1177/1687814017750434.
[19] AKGUN M., KARA F., 2021, *Analysis and Optimization of Cutting Tool Coating Effects on Surface Roughness and Cutting Forces on Turning of Aa 6061 Alloy,* Adv. Mater. Sci. Eng., https://doi.org/10.1155/2021/6498261.
[20] ASLAN A., 2020, *Optimization and Analysis of Process Parameters for Flank Wear, Cutting Forces and Vibration in Turning of AISI 5140:* A Comprehensive Study, Measurement, 163, https://doi.org/10.1016/J.Measurement. 2020.107959.
[21] YANG S H. NATARAJAN U., 2010, *Multi-Objective Optimization of Cutting Parameters in Turning Process Using Differential Evolution and Non-Dominated Sorting Genetic Algorithm-II Approaches,* Int. J. Adv. Manuf. Technol., 49/5–8, 773–784.
[22] MALI H.S., UNUNE D.R., NIRALA C.K., 2018. *ANN-NSGA-II Dual Approach for Modeling and Optimization in Abrasive Mixed Electro Discharge Diamond Grinding of Monel K-500.* Engineering Science and Technology, an International Journal, 21/3, 322–329, https://doi.org/10.1016/j.jestch.2018.04.014.
[23] CYDAS U., 2010, *Machinability Evaluation in Hard Turning of AISI 4340 Steel with Different Cutting Tools Using Statistical Techniques*, Proc. Inst. Mech. Eng. Part B, J. Eng. Manuf., 224/7, 1043–1055.
[24] KALADHA M.R, 2020, *Modeling and Optimization for Surface Roughness and Tool Flank Wear in Hard Turning of AISI 4340 Steel (35 HRC) Using TiSiN-TiAlN Nanolaminate Coated Insert,* Multidiscip. Model. Mat. Struct., 17/2, 337–359, https://doi.org/10.1108/MMMS-12-2019-0217.
[25] PATOLE P.B., KULKARNI V.V., 2018, *Optimization of Process Parameters Based on Surface Roughness and Cutting Force in MQL Turning of AISI 4340 Using Nano Fluid,* Mater. Today Proc., 5/1 104–112.
[26] GUPTA M.K., SOOD P.K., 2015, *Optimization of Machining Parameters for Turning AISI 4340 Steel Using Taguchi Based Grey Relational Analysis*, Materials Science, Business, Corpus ID: 13750423.
[27] DAS S.R., PANDA A., DHUPAL D., 2017, *Experimental Investigation of Surface Roughness, Flank Wear, Chip Morphology and Cost Estimation During Machining of Hardened AISI 4340 Steel with Coated Carbide Insert,* Mech. Adv. Mater. Mod. Process., 3/1, 1–14.
[28] CORTES C., VAPNIK V., 1995, *Support-Vector Networks,* Mach. Learn., 20, 273–297, http://dx.doi.org/10.1007/ BF00994018.
[29] KHAN P.W., BYUN Y.-C., LEE S.-J., KANG D.-H., KANG J.-Y., PARK H.-S., 2020, *Machine Learning-Based Approach to Predict Energy Consumption of Renewable and Nonrenewable Power Sources,* Energies, 13/18, 4870.
[30] [DOROGUSH A.V., ERSHOV V., GULIN A., 2018, *Catboost: Gradient Boosting with Categorical Features Support,* ArXiv Prepr. ArXiv181011363.
[31] HUANG G. et al., 2019, *Evaluation of Catboost Method for Prediction of Reference Evapotranspiration in Humid Regions,* J. Hydrol., 574, 1029–1041.
[32] ZHANG Y., MA J., LIANG S., LI X., LI M., 2020, *An Evaluation of Eight Machine Learning Regression Algorithms for Forest Aboveground Biomass Estimation From Multiple Satellite Data Products,* Remote Sens., 12/24, 4015.
[33] MAIMON O.Z., ROKACH L., 2014, *Data Mining with Decision Trees: Theory and Applications,* World Scientific, 81, https://doi.org/10.1142/9097.
[34] FLORES V., KEITH B., 2019, *Gradient Boosted Trees Predictive Models for Surface Roughness in High-Speed Milling in the Steel and Aluminum Metalworking Industry,* Complexity, https://doi.org/10.1155/2019/1536716.
[35] HUANG B.P., CHEN J.C., LI Y., 2008, *Artificial-Neural-Networks-Based Surface Roughness Pokayoke System for End-Milling Operations,* Neurocomputing, 71/4–6, 544–549.
[36] KARA F., ASLANTAS K., CICEK A., 2015, *Ann and Multiple Regression Method-Based Modelling of Cutting Forces in Orthogonal Machining of Aisi 316l Stainless Steel,* Neural Comput. Appl., 26/1, 237–250, https://doi.org/10.1007/S00521-014-1721-Y.
[37] KARA F., ASLANTAŞ K., CICEK A., 2016, *Prediction of Cutting Temperature in Orthogonal Machining of AISI 316L Using Artificial Neural Network,* Appl. Soft Comput., 38, 64–74, https://doi.org/10.1016/J.Asoc.2015.09.034.
[38] NGUYEN V.-H., LE T.-T., TRUONG H.-S., DUONG H.T., LE M.V., 2023, *Predicting Volumetric Error Compensation for Five-Axis Machine Tool Using Machine Learning,* Int. J. Comput. Integr. Manuf., 1–28, https://doi.org/10.1080/0951192x.2022.2163295.

[39] NGUYEN V.-H., LE T.-T., 2022, *Developing Geometric Error Compensation Software for Five-Axis CNC Machine Tool on NC Program Based on Artificial Neural Network*, Advances in Asian Mechanism and Machine Science, Cham, 541–548, https://doi.org/10.1007/978-3-030-91892-7_51.
[40] DEB K., PRATAP A., AGARWAL S., MEYARIVAN T., 2002, *A Fast and Elitist Multiobjective Genetic Algorithm: NSGA-II*, IEEE Trans. Evol. Comput., 6/2, 182–197.
[41] COELLO C.A.C., LAMONT G.B., Van VELDHUIZEN D.A., 2007, *Evolutionary Algorithms for Solving Multi-Objective Problems*, Springer New York, NY.
[42] INJADAT M., MOUBAYED A., NASSIF A.B., SHAMI, A. 2020, *Systematic Ensemble Model Selection Approach for Educational Data Mining*, Knowl.-Based Syst., 200, 105992, https://doi.org/10.1016/j.knosys.2020.105992.
[43] RASHID W.B., GOEL S., DAVIM J.P., JOSHI S.N., 2016, *Parametric Design Optimization of Hard Turning of AISI 4340 Steel (69 HRC)*, Int. J. Adv. Manuf. Technol., 82/1–4, 451–462.
[44] DENNISON M.S., SIVARAM N.M., BARIK D., PONNUSAMY S., 2019, *Turning Operation of AISI 4340 Steel in Flooded, Near-Dry and Dry Conditions: a Comparative Study on Tool-Work Interface Temperature*, Mech. Mech. Eng., 23/1. 172–182.